THE JOURNAL OF BIOLOGICAL CHEMISTRY
Vol. 276, No. 48, Issue of November 30, pp. 45079–45087, 2001
Printed in U.S.A.

Solution Structure of a Kunitz-type Chymotrypsin Inhibitor Isolated from the Elapid Snake *Bungarus fasciatus**

Received for publication, July 3, 2001, and in revised form, August 17, 2001
Published, JBC Papers in Press, September 18, 2001, DOI 10.1074/jbc.M106182200

Chinpan Chen‡§, Chun-Hua Hsu‡¶, Ning-Yuan Su‡, Yu-Ching Lin‖, Shyh-Horng Chiou¶‖, and Shih-Hsiung Wu¶‖‡‡**

From the Institutes of ‡Biomedical Sciences and ‖Biological Chemistry, Academia Sinica, Taipei 115, Taiwan and the ¶Institute of Biochemical Sciences, National Taiwan University, Taipei 106, Taiwan

Bungarus fasciatus **fraction IX (BF9), a chymotrypsin inhibitor, consists of 65 amino acid residues with three disulfide bridges. It was isolated from the snake venom of *B. fasciatus* by ion-exchange chromatography and belongs to the bovine pancreatic trypsin inhibitor (BPTI)-like superfamily. It showed a dissociation constant of 5.8×10^{-8} M with α-chymotrypsin as measured by a BIAcore binding assay system. The isothermal titration calorimetry revealed a 1:1 binding stoichiometry between this inhibitor and chymotrypsin and apparently no binding with trypsin. We further used CD and NMR to determine the solution structure of this venom-derived chymotrypsin inhibitor. The three-dimensional NMR solution structures of BF9 were determined on the basis of 582 restraints by simulated annealing and energy minimization calculations. The final set of 10 NMR structures was well defined, with average root mean square deviations of 0.47 Å for the backbone atoms in the secondary structure regions and 0.86 Å for residues The side chains of Phe^{23}, Tyr^{24}, Tyr^{25}, Phe^{35}, and Phe^{47} exhibited many long-range nuclear Overhauser effects and were the principal components of the hydrophobic core in BF9. To gain insight into the structure-function relationships among proteins in the BPTI-like superfamily, we compared the three-dimensional structure of BF9 with three BPTI-like proteins that possess distinct biological functions. These proteins possessed similar secondary structure elements, but the loop regions and β-turn were different from one another. Based on residues at the functional site of each protein, we suggest that the flexibility, rigidity, and variations of the amino acid residues in both the loop and β-turn regions are related to their biological functions.**

Proteins that belong to the bovine pancreatic trypsin inhibitor (BPTI)[1]-like superfamily are present in a variety of living organisms. They display significant differences in amino acid sequences and in biological functions, but they all possess three disulfide bridges, which supposedly contribute to the overall stability of this class of proteins. In general, the BPTI-like superfamily is classified into two families based on protein structure: (*a*) small Kunitz-type inhibitors and BPTI-like toxins and (*b*) soft tick anticoagulant proteins.

To date, structural studies have been extensively carried out on the BPTI-like superfamily proteins. For small Kunitz-type inhibitors, a number of x-ray crystal structures (1, 2) as well as the solution structure of BPTI (3) have been reported. Both NMR and x-ray three-dimensional structures of the human Kunitz-type protease inhibitor domain of the Alzheimer's amyloid β-protein precursor (4, 5) have been solved, as have the NMR solution structures of the Kunitz-type domain from the human type VI collagen α3(VI) chain (C5) (6) and of a Kunitz-type protease inhibitor from the sea anemone *Stichodactyla helianthus* (7). Most BPTI-like toxins isolated from snake venom are Ca^{2+} or K^+ channel blockers, *e.g.* α-dendrotoxin, dendrotoxin K (DTK), dendrotoxin I, calcicludine, and the smaller subunit of β-bungarotoxin from various snake sources (8, 9). The three-dimensional structures of these BPTI-like toxins have been determined using NMR and/or x-ray crystallography (10–13). In the family of soft tick anticoagulant proteins, the NMR solution structure of tick anticoagulant protein (TAP), a highly selective inhibitor of blood coagulation factor Xa that exhibits no inhibitory activity against other common serine proteases such as trypsin, chymotrypsin, or thrombin, has been solved (14, 15). Ornithodorin, a potent and highly selective thrombin inhibitor, also belongs to this family, and the ornithodorin-thrombin complex crystal structure has been reported (16).

Bungarus fasciatus fraction IX (BF9), which consists of 65 amino acid residues with three disulfide bridges, is the fraction IX component isolated from the venom of *B. fasciatus*. It is a Kunitz-type protease inhibitor that possesses inhibitory action only against chymotrypsin and belongs to the BPTI-like superfamily (17). Fig. 1 shows the sequence alignments of BF9 with seven other proteins in the BPTI-like superfamily, including three small Kunitz-type inhibitors (BPTI, C5, and *S. helianthus* proteinase inhibitor), three BPTI-like toxins (dendrotoxin I, DTK, and calcicludine), and a soft tick anticoagulant protein (TAP). The sequence identity of BF9 to the Kunitz-type inhibitors and BPTI-like toxins is ~35–50%, but the sequence iden-

* This work was supported by Academia Sinica and the National Science Council (Taipei, Taiwan). The costs of publication of this article were defrayed in part by the payment of page charges. This article must therefore be hereby marked "*advertisement*" in accordance with 18 U.S.C. Section 1734 solely to indicate this fact.

The atomic coordinates and structure factors (code 1JC6) have been deposited in the Protein Data Bank, Research Collaboratory for Structural Bioinformatics, Rutgers University, New Brunswick, NJ (http://www.rcsb.org/).

The resonance assignment of BF9 at 310 K and pH 3.0 has been deposited in the BioMagResBank under accession number 5050.

§ To whom correspondence may be addressed: Inst. of Biomedical Sciences, Academia Sinica, 128 Academia Rd., Section 2, Taipei 115, Taiwan. Tel.: 886-2-2652-3035; Fax: 886-2-2788-7641; E-mail: bmchinp@ccvax.sinica.edu.tw.

** To whom correspondence may be addressed: Inst. of Biological Chemistry, Academia Sinica, 128 Academia Rd., Section 2, Taipei 115, Taiwan. Tel.: 886-2-2785-5696 (Ext. 7010); Fax: 886-2-2653-0014; E-mail: shchiou@gate.sinica.edu.tw.

‡‡ To whom correspondence may be addressed: Inst. of Biological Sciences, Academia Sinica, 128 Academia Rd., Section 2, Taipei 115, Taiwan. Tel.: 886-2-2785-5696 (Ext. 7101); Fax: 886-2-2653-9142; E-mail: shwu@gate.sinica.edu.tw.

[1] The abbreviations used are: BPTI, bovine pancreatic trypsin inhibitor; DTK, dendrotoxin K; TAP, tick anticoagulant protein; BF9, *B. fasciatus* fraction IX; TOCSY, total correlation spectroscopy; NOESY, nuclear Overhauser effect correlation spectroscopy; NOE, nuclear Overhauser effect.

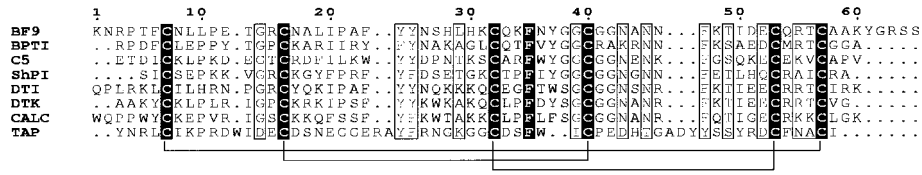

FIG. 1. **Sequence of BF9 aligned with those of seven BPTI-like superfamily proteins for which three-dimensional solution structures have been determined.** These are BPTI (3), C5 (6, 37), the *S. helianthus* proteinase inhibitor (*ShPI*) (7), dendrotoxin I (*DTI*) (12), DTK (11), calcicludine (*CALC*) (13), and TAP (15). The three disulfide bridges are shown by *brackets*.

tity between BF9 and TAP is much smaller (13.3%). Laskowski and Kato (18) pointed out that the P1 site residue in the trypsin inhibitor is a positively charged residue (Arg or Lys) and in the chymotrypsin inhibitor usually is a large hydrophobic residue (Leu, Phe, or Tyr). The P1 reactive-site residue of BF9 has been identified, however, to be Asn^{17} (17). Recently, the P1 site residues His and Asn for chymotrypsin binding were also reported (19). It is therefore interesting to know the structural differences that are responsible for the distinct biological functions among the proteins in the BPTI-like superfamily. The Kunitz-type protease inhibitor possessing specific chymotrypsin inhibition is very rare, and the detailed three-dimensional structure of this kind of protease inhibitor has not yet been reported. In this work, we used surface plasmon resonance and isothermal titration calorimetry to obtain the binding constant for BF9 and α-chymotrypsin. In addition, we applied CD and NMR techniques to determine the solution structure of BF9. We then made a structural comparison between BF9 and BPTI, DTK, and TAP to shed some light on structure-function relationships in these homologous proteins with distinct functions.

EXPERIMENTAL PROCEDURES

Sample Preparation—BF9 was isolated and purified from the snake venom of *B. fasciatus* by ion-exchange chromatography on CM-cellulose and by gel filtration on Sephadex G-50 (17). Unless otherwise stated, all reagents and solvents were obtained commercially as reagent grade and used without further purification.

Surface Plasmon Resonance—Association and dissociation of BF9 and α-chymotrypsin were measured with a BIAcore X instrument (BIAcore AB, Uppsala, Sweden). BF9 was coupled to a carboxymethyldextran CM5 sensor chip with an amine coupling kit containing *N*-ethyl-*N*′-(3-dimethylaminopropyl)carbodiimide HCl, ethanolamine HCl, and *N*-hydroxysuccinimide. After the chip was activated by 35 μl of *N*-ethyl-*N*′-(3-dimethylaminopropyl)carbodiimide HCl/*N*-hydroxysuccinimide mixture, BF9 was coupled to the CM5 sensor surface using 35 μl of BF9 (5 μM) in BIAcore binding buffer (10 mM HEPES, 150 mM NaCl, and 3 mM EDTA (pH 7.4) containing 0.005% surfactant P_2O). The binding assay was performed with a constant flow rate of 30 μl/min at 25 °C with α-chymotrypsin concentrations in the range of 10–500 nM. 5 M NaCl was used to regenerate the chip. For fitting of the binding kinetics, BIAevaluation Version 3.0 software (BIAcore AB) was applied, and the 1:1 Langmuir binding model was chosen.

Isothermal Titration Calorimetry—Titration calorimetry experiments were performed with a VP-ITC titration calorimetric system (Microcal Inc., Northampton, MA). 0.04 mM BF9 solution in 20 mM HEPES (pH 7.5) in the calorimetric cell was titrated with 0.3 mM α-chymotrypsin dissolved in the same buffer in a 250-μl injection syringe at 30 °C. The raw calorimetry data were collected and analyzed by Origin Version 5.0 data analysis software (Microcal Inc.). The binding isotherms were fitted to the one-site binding model, giving values for the stoichiometry (*N*) of the interaction, the enthalpy of binding (Δ*H*), and the binding constant (*K*).

CD Experiments—CD experiments were carried out using an Aviv 202 instrument (Aviv, Lakewood, NJ) calibrated with (+)-10-camphorsulfonic acid at 25 °C. In general, a 2-mm path-length cuvette with 20 μM BF9 peptide in 20 mM phosphate buffer was used for CD experiments, and all protein solutions were made up to 1 ml. The CD spectra of BF9 at different temperatures and pH values were recorded. Each of the CD spectra was obtained from an average of three scans with 1-nm bandwidth. The spectra were recorded from 180 to 260 nm at a scanning rate of 38 nm/min with a wavelength step of 0.5 nm and a time constant of 100 ms. After background subtraction and smoothing, all the CD data were converted from CD signal (millidegree) into mean residue ellipticity (degrees cm^2 $dmol^{-1}$). The secondary structure content was estimated from the CD spectra according to the methods of CONTIN-LL, SELCON3, and CDSSTR (20).

NMR Experiments—The NMR measurements were carried out on a Bruker AMX-500 or AVANCE-600 spectrometer (Bruker, Karlsruhe, Germany). Samples for NMR experiments contained 0.35 ml of 2 mM BF9 in 50 mM phosphate buffer at pH 3.0, 3.9, and 7.0. pH values were measured with a dissolved-oxygen (DO) microelectronic pH-vision Model PHB-9901 pH meter equipped with a 4-mm electrode. All reported pH values were direct readings from the pH meter without correction for isotope effect. For monitoring the exchange rates of labile protons, the concentrated sample in H_2O was lyophilized only once and redissolved in D_2O (99.99% D). NMR spectra were acquired immediately and thereafter at appropriate time intervals. All chemical shifts were externally referenced to the methyl resonance of 2,2-dimethyl-2-silapentane-5-sulfonate (0 ppm). Double quantum filtered COSY (21), TOCSY (22), and NOESY (23) spectra were collected with 512 t_1 increments and 2048 complex data points. All spectra were recorded in time-proportional phase-sensitive mode (24). Low temperature studies employed a temperature-controlled stream of cooled air using a Bruker BCU refrigeration unit and a B-VT 2000 control unit. Water suppression was achieved by 1.4 s of pre-saturation at the water frequency or by the gradient method (25). All spectra were collected with 6024.1- and 7788.16-Hz spectral widths for AMX-500 and AVANCE-600, respectively.

The data were transferred to an SGI O_2 200-MHz R5000SC work station (Silicon Graphics, Mountain View, CA) for all processing and further analysis using the Bruker XWINNMR and AURELIA software packages. All data sets acquired were zero-filled to equal points in both dimensions prior to further processing. A 60°-shifted skewed sine bell window function was used for all NOESY and TOCSY spectra and a 20°- or 30°-shifted skewed sine bell function was used for all COSY spectra. To help with resolving spectral overlap, data were collected at different temperatures.

Torsional Angle Restraints and Stereospecific Assignment—The $^3J_{NH\alpha}$ coupling constants were estimated from the residual intensity of the anti-phase cross-peak in double quantum filtered COSY spectra recorded in H_2O. φ torsional restraints of −130 ± 30° for $^3J_{NH\alpha}$ coupling constants >8 Hz and −60 ± 30° for $^3J_{NH\alpha}$ coupling constants <6 Hz were used for structure calculation. We obtained a total of 20 φ torsional restraints mainly located in the α-helix and β-strand regions. The φ torsional restraints were used for structure generations starting from the early stage when NOE correlations were also consistent. The stereospecific assignments were derived using the method of Hyberts *et al.* (26). The stereospecific assignment of β-methylene allowed us to assign the χ_1 torsional angle restraints to 60 ± 30°, 180 ± 30°, or −60 ± 30°. To ensure the accuracy of stereospecific assignments, we obtained only 13 prochiral assignments with certainty. We found that the stereospecific assignments agreed well with our generated structures in the early stage. Thus, in the later stage of structure generation, we also added χ_1 and prochiral assignments as restraints in the structure calculation.

Hydrogen Bond and Disulfide Restraints—The amide proton exchange rates were identified from residual amide proton signals observed in several TOCSY spectra recorded at 310 K and pH 3.0 and 7.0. The first spectrum was recorded within 5 h after the lyophilized sample was redissolved in D_2O. The amide proton exchange rates were categorized into three classes: fast, medium, and slow. Hydrogen bond formation or solvent exclusion from the amide protons was assumed to account for the slow and medium exchanging amide protons. Most of these protons have been identified to be associated with particular secondary structures. For better convergence, a number of hydrogen bonds involved in the secondary structure were included as distance restraints in the final stage of structure generation, *i.e.* an O–N distance of between 2.5 and 3.3 Å and O–HN distances of 1.8 and 2.5 Å between NH protons and the backbone carbonyl oxygen atoms were assigned to the slow and medium exchanging protons, respectively, in the latter stage

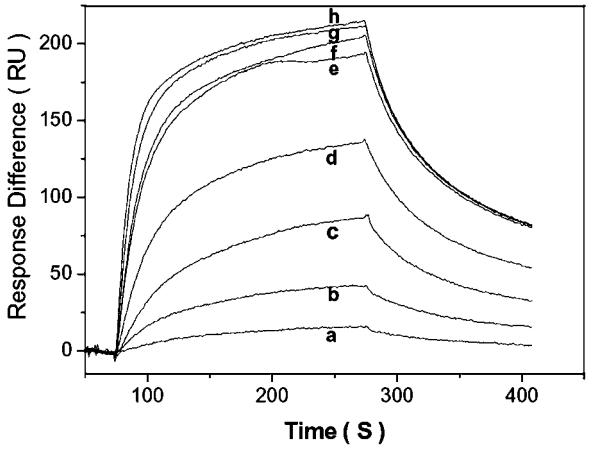

FIG. 2. **Representative overlaid sensorgram for kinetic study of α-chymotrypsin binding to BF9 measured by a BIAcore X system.** BF9 was immobilized on a CM5 sensor chip by amine coupling. The α-chymotrypsin was injected over the sensor chip at concentrations ranging from 10 to 500 nM: *trace a*, 10 nM; *trace b*, 30 nM; *trace c*, 50 nM; *trace d*, 100 nM; *trace e*, 200 nM; *trace f*, 300 nM; *trace g*, 400 nM; *trace h*, 500 nM. Raw binding data were analyzed by BIAevaluation Version 3.0 Software and fit to a 1:1 Langmuir binding model. *RU*, response units.

of structure determination. In the final stage of structure calculation, the hydrogen bonds between NH_i and OC_j in the β-sheet structures were included as restraints only if the β-sheet inter-strand NH_i/NH_j, $NH_i/C^{\alpha}H_{j+1}$, and $C^{\alpha}H_{i-1}/C^{\alpha}H_{j+1}$ NOE cross-peaks were observed. The disulfide bonds used in the structure calculation were Cys^{7}–Cys^{57}, Cys^{16}–Cys^{40}, and Cys^{32}–Cys^{53}. Covalent bonds between the sulfur atoms of disulfide bridges were modeled by restraining the distances between the two sulfur atoms to 1.80–2.30 Å.

Tertiary Structure Calculations—Distance restraints of BF9 were derived primarily from the 200-ms NOESY spectrum recorded in the aqueous solution at 310 K and pH 3.0. Comparison was made with the 100-ms NOESY spectrum to assess possible contributions of the NOEs from spin diffusion. Peak intensities were classified as large, medium, small, and very small, corresponding to upper bound inter-proton distance restraints of 2.5, 3.5, 4.5, and 6.0 Å, respectively. An additional correction of 1.0 Å was added for methylene and methyl groups. Backbone dihedral restraints were inferred from $^{3}J_{NH\alpha}$ coupling constants, with ϕ restrained to $-130 \pm 30°$ for $^{3}J_{NH\alpha} > 8$ Hz and $-60 \pm 30°$ for $^{3}J_{NH\alpha} < 6$ Hz. The structure determination was performed using 517 distance restraints, of which 127 were intra-residue, 172 were sequential, and 218 were medium- and long-range inter-proton distances; and 63 were additional restraints, including 32 hydrogen bonds, 20 ϕ torsional angles, and 13 χ_1 torsional angles. All simulated minimization and dynamic annealing calculations were carried out with the program X-PLOR Version 98 (27) on an SGI O_2 work station. The Insight II (Molecular Simulation Inc., San Diego, CA), MOLMOL (28), and GRASP (29) programs were used to visually observe sets of structures and to calculate and make the electrostatic surface potential of the final three-dimensional models. The distributions of the backbone dihedral angles of the final converged structures were evaluated by the representation of the Ramachandran dihedral pattern, revealing the deviations from the sterically allowed (ϕ, ψ) angle limits using MOLMOL and PROCHECK-NMR (30).

RESULTS

Binding Studies with α-Chymotrypsin—To determine the dissociation constant for BF9 with α-chymotrypsin, surface plasmon resonance measurements were carried out. BF9 was coupled to a carboxymethyl-dextran CM5 sensor chip with an amine coupling kit. Binding was observed upon injection of different concentrations of α-chymotrypsin (Fig. 2). The plateau values reached after completion of the association reaction were analyzed by a Langmuir binding isotherm. A dissociation constant of 5.8×10^{-8} M was obtained. Another complementary method used to study the binding of BF9 to α-chymotrypsin was isothermal titration calorimetry. Fig. 3 shows the experimental data for titration of BF9 with α-chymotrypsin using

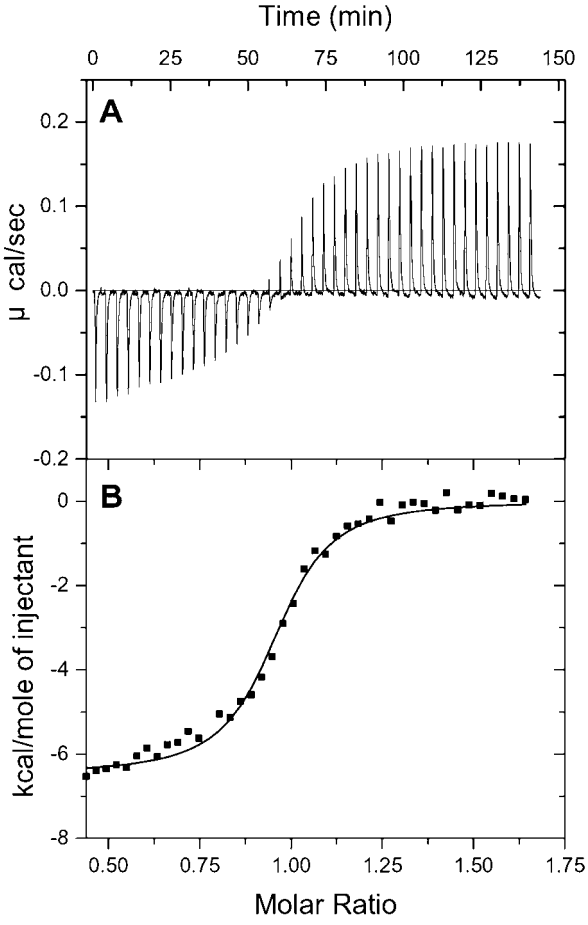

FIG. 3. **Isothermal titration calorimetry data of BF9 titrated with α-chymotrypsin.** Experiments were carried out in an VP-ITC system at 30 °C with stirring at 300 rpm. *A*, raw data in microcalories/s *versus* time showing heat release upon injections of 0.3 mM α-chymotrypsin into a 1.4-ml cell containing 0.04 mM BF9; *B*, integration of the raw data yields the heat/mol *versus* molar ratio. The best values of the fitting parameters are 0.95 for *N*, 4.3×10^{6} M^{-1} for *K*, and −6.45 kcal/mol for ΔH.

isothermal titration calorimetry. The analysis of the data revealed a 1:1 stoichiometry of the two binding partners, a K_d value of 2.3×10^{-7} M, and an apparent ΔH of −6.45 kcal/mol. There is apparently no binding between BF9 and trypsin as measured by the same assay system.

BF9 Is a Highly Stable Protease Inhibitor—We performed CD experiments on BF9 at different pH values (pH 3.5–7.0) and at different temperatures (0–80 °C). We found that BF9 possessed similar conformations at different pH values. The CD spectra from 0 to 80 °C at pH 3.5, as shown in Fig. 4, revealed a decrease in negative band intensity when the temperature was increased, whereas the minimum stayed almost the same at 203 nm. This indicated that the majority of the secondary structure still existed even at 80 °C. Thus, BF9 is a highly thermostable protein, similar to BPTI, which has a denaturation temperature ≥95 °C at pH 4.6 (6). The contents of the secondary structures of BF9 estimated using CONTIN-LL, SELCON3, and CDSSTR (20) are listed in Table I. The contents are comparable, and the average contents of the α-helix, β-strand, β-turn, and unordered forms are 17.9, 22.7, 24.2, and 35.2%, respectively.

Resonance Assignments and Secondary Structure Determination—With high thermostability and well dispersed NMR data, BF9 is an excellent candidate for NMR structural studies. Initially, we carried out NMR studies at neutral pH. We could not obtain confident and complete resonance assignments due

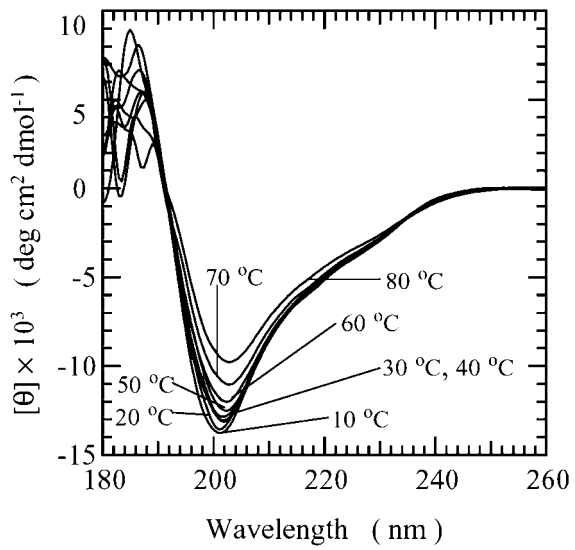

FIG. 4. **CD spectra of 20 μM BF9 in 20 mM phosphate buffer at pH 3.5 shown as a function of temperature.** *deg*, *degrees.*

to several missing backbone and side chain amide protons, presumably due to their fast exchange with H_2O. To lower the exchange rate, we performed NMR experiments at pH 3.9 and 3.0, and the missing protons all appeared and were identified. Based on the NMR data acquired at different pH values and temperatures, the resonance assignments were accomplished using the standard procedures (31), in which spin systems were identified based on COSY and TOCSY experiments, and sequential connectivities were obtained from NOESY experiments.

The fingerprint region of a well resolved TOCSY spectrum with partial annotation is shown in Fig. 5. We met with several difficulties when assigning resonance due to the presence of the same chemical shifts for both $C^{\alpha}H$ and $C^{\beta}H$ in Thr^5 and of a higher $C^{\beta}H$ chemical shift (4.03 ppm) than a $C^{\alpha}H$ chemical shift (3.77 ppm) in Ser^{27}. Table II lists the nearly complete chemical shift assignments for BF9 at 310 K and pH 3.0. We found several unusual chemical shifts. For example, $C^{\alpha}H$ protons of Cys^{53} and Ile^{50} possessed upfield shifts at 1.89 and 3.05 ppm, respectively. We observed the amide proton of Tyr^{25} at a downfield shift of 10.55 ppm and identified $C^{\beta}H_2$ (0.24 and 0.47 ppm) and $C^{\gamma}H_2$ (0.38 and 0.67 ppm) of Pro^{11} in the upfield regions. Interestingly, we also found these unusual shifts, with the exception of H^N (Phe^{26}) and $C^{\beta}H_2$ (Tyr^{52}) in TAP, in the corresponding residues of other BPTI-like proteins.

Fig. 6 shows the summary of the NMR parameters for BF9 at pH 3.0. The $C^{\alpha}H$ chemical shift index indicated that Arg^3–Lys^7 and Ile^{50}–Ala^{58} formed α-helical structures and that Leu^{19}–Tyr^{24}, Lys^{31}–Tyr^{37}, and Asn^{45}–Thr^{49} exhibited β-strand conformations. Based on the α-helical NOEs, we observed a regular α-helix in the C-terminal Ile^{50}–Cys^{57} segment, which was in good agreement with chemical shift index results. The chemical shift index method also predicted the existence of an α-helix in the N-terminal Arg^3–Lys^7 segment. However, we observed only an α-helical NOE, $d_{\alpha N}$ (6, 9), in this segment, indicating that this region likely forms a turn-like or 3_{10} helix conformation. According to the observed long-range NOEs and the deduced hydrogen bonds consistent with the β-sheet structure, as shown in Fig. 7, we identified that a double-stranded antiparallel β-sheet, spanning Ala^{22}–Asn^{26} for the first strand and Lys^{31}–Asn^{36} for the second, occupies a central place in the sequence. Furthermore, we observed a β-turn conformation in Ser^{27}–His^{30} between the β_1- and β_2-strands. By contrast, there were only three inter-residue NOEs between β_1 and β_3. Among these crossover NOEs, $d_{\alpha N}$ (24, 47) and $d_{\alpha\alpha}$ (24, 46) were present only at a higher mixing time, and their intensities were very weak. Therefore, it is likely that only Phe^{47} associated with Phe^{23} to form a one-residue third strand in an antiparallel manner, which is a feature that was previously reported for other proteins in the BPTI-like superfamily.

We observed an intensive $d_{\alpha\delta(i,\, i+1)}$ NOE for all three proline residues (Pro^4, Pro^{11}, and Pro^{21}) in BF9, indicating that the *trans*-conformation is predominant. To check the rigidity and to identify the hydrogen bonds, we carried out an amide proton exchange study of BF9 at 310 K and pH 3.0 and 7.0. We observed 22 amide protons at pH 3.0 (Asn^8, Leu^9, Ile^{20}, Ala^{22}, Phe^{23}, Tyr^{24}, Tyr^{25}, Asn^{26}, His^{30}, Lys^{31}, Gln^{33}, Phe^{35}, Asn^{45}, Asn^{46}, Phe^{47}, Thr^{49}, Cys^{53}, Gln^{54}, Arg^{55}, Thr^{56}, Cys^{57}, and Ala^{58}) that possessed medium or slow exchange rates. By contrast, only 10 amide protons at pH 7.0 (Phe^{23}, Tyr^{24}, Tyr^{25}, Asn^{26}, Lys^{31}, Gln^{33}, Phe^{35}, Phe^{47}, Cys^{53}, and Gln^{54}) showed medium and slow exchange rates. These residues with medium and slow amide proton exchange rates were all located in polypeptide segments for which the spatial structure was well defined by the NMR data. The residues are mostly amide protons that form characteristic hydrogen bonds in the regular secondary structure elements. Comparison of the exchange rate data revealed that the two β-strands, the one-residue third β-strand at Phe^{47}, and the C-terminal α-helix at Ile^{50}–Gln^{54} possessed high stability based on our observation of slow exchange rates in these regions at both pH values.

Three-Dimensional Solution Structure of BF9—A set of 582 restraints was used for simulated annealing and energy minimization calculations using the program X-PLOR. Among these restraints, 517 were inter-proton distances, 32 were hydrogen bonds, and 33 were dihedral angles. Ten structures with the lowest target function and minimal distance and torsional angle restraint violations in the final stage were chosen to represent the ensemble of NMR structures. These structures were consistent with both experimental data and standard covalent geometry and displayed no violations >0.5 Å for distance restraints. Superposition of each structure with the mean structure yielded average root mean square deviations 0.86 Å for the backbone atoms in residues 3–58 and 0.47 Å for the backbone atoms in the well defined secondary structure regions Pro^{21}–Asn^{26}, Lys^{31}–Asn^{36}, and Ile^{50}–Cys^{57}, as shown in Fig. 8*A*. Due to the presence of fewer NOE distance restraints, the loop regions (Glu^{12}–Leu^{19} and Gly^{38}–Ala^{44}) are less well defined, as shown in Fig. 8*B*. The residues in these loop regions all possess fast amide proton exchange rates, further indicating a high flexibility in these regions.

The structural statistics on the final set of structures are given in Table III. Analysis of the ensemble of 10 structures using PROCHECK-NMR revealed that 97% of the residues lie in the most favored and additional allowed regions of the Ramachandran ϕ/ψ dihedral angle plot (Fig. 9). The distribution of ϕ, ψ, and χ_1 dihedral angles (data not shown) further demonstrated the rigidity of the secondary structure regions. The solution structures of BF9 depict the well known Kunitz-type inhibitor fold. The core of the domain, comprising the secondary structure elements and two of the three disulfide bonds (Cys^7–Cys^{57} and Cys^{32}–Cys^{53}), was exceptionally well defined. The side chains of Phe^{23}, Tyr^{24}, Tyr^{25}, Phe^{35}, and Phe^{47} exhibited an extremely large number of long-range NOEs, and close inspection of the three-dimensional structure revealed that these residues are the principal components of the hydrophobic core in BF9.

Hydrogen Bond Networks and Surface Structure—An examination of the atomic positions in the above 10 solution structures provides information about the hydrogen bonds. In this

TABLE I
Secondary structure contents of BF9 estimated from CD spectrum acquired at pH 3.5 and 30 °C using three different methods

Methods	α_R [a]	α_D	β_R	β_D	T	U
CONTIN-LL	0.055	0.122	0.115	0.095	0.262	0.351
SELCON3	0.081	0.114	0.134	0.087	0.228	0.362
CDSSTR	0.045	0.120	0.163	0.090	0.237	0.345

[a] α_R, regular α-helix; α_D, distorted α-helix; β_R, regular β-strand; β_D, distorted β-strand; T, turns; U, unordered.

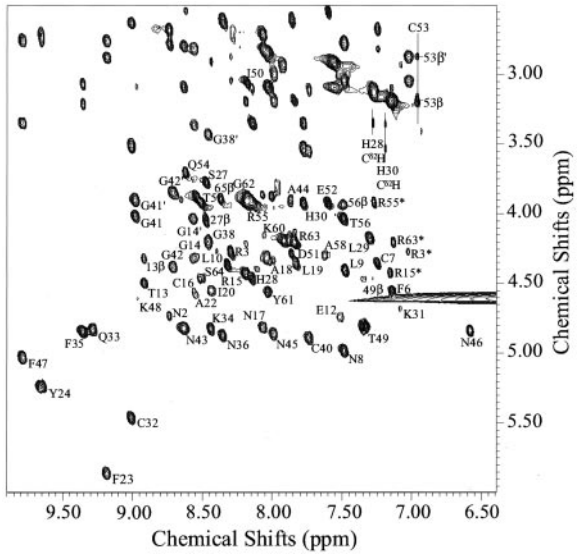

FIG. 5. **Fingerprint region of a TOCSY spectrum of BF9 acquired at 310 K and pH 3.0.** The assignments are indicated by one-letter amino acid codes and residue numbers. The $C^{\alpha}H$ of Cys^{53} located at 1.89 ppm is not shown in the spectrum, and $C^{\beta}H_2$ is labeled instead. The side chain $N^{\epsilon}H/C^{\alpha}H$ cross-peaks of Arg residues are labeled with *asterisks*. The side chain $C^{\delta 2}H/C^{\beta}H_2$ cross-peaks of His^{28} and His^{30} are also annotated.

regard, one hydrogen bond was considered to be formed if the hydrogen distance to the acceptor atom was <2.5 Å and the O-H-N angle was >125°. Table IV lists the backbone–backbone hydrogen bonds identified in >30% of the 10 NMR solution structures. Most of the hydrogen bonds are situated in the β-sheet and C-terminal α-helix regions, with some of the hydrogen bonds located outside of well defined secondary structure regions. For example, in the N-terminal region, we identified two hydrogen bonds, Asn^8 NH–Thr^5 CO and Leu^9 NH–Phe^6 CO. The formation of two hydrogen bonds at Asn^8 and Leu^9 is consistent with exchange rate results showing that Asn^8 and Leu^9 possess a medium and slow exchange rate, respectively (see Fig. 6). Also, it further indicated that the N-terminal Thr^5–Leu^9 segment formed a 3_{10} α-helical conformation. In the β-turn region (Ser^{27}–His^{30}), we saw two hydrogen bonds, His^{30} NH–Asn^{26} CO and His^{30} NH–Ser^{27} CO. BF9 is a basic protein (pI 9.22) with four arginine, five lysine, one aspartate, and two glutamate residues. At neutral pH, it carries an overall positive charge, but the distribution of the charge is highly asymmetric. There are two groups of positively charged side chains situated close to each other at the "base" of the molecule: one close to the N terminus (Lys^1 and Arg^3) and the other in the second β-strands (Lys^{31} and Lys^{34}). There are also several uncompensated positive charges scattered over the surface of the molecule (Arg^{15} and Lys^{48}).

DISCUSSION

Using surface plasmon resonance and isothermal titration calorimetry, we confirmed that there is characteristic and specific binding between BF9 and chymotrypsin. In contrast, the binding property was not observed between BF9 and trypsin under the same conditions using both approaches. The discrepancy in the dissociation constant values measured by BIAcore binding assay and isothermal calorimetry is probably due to different buffers used in these two methods. We found that reproducibility was greater in the BIAcore assay system compared with calorimetry. On the other hand, the binding stoichiometry was easier to obtain by the calorimetry method. These two methods were complementary in our study of the binding constant. Therefore, we believe that the value of 5.8×10^{-8} M obtained by BIAcore binding assays is more accurate than the valued obtained by isothermal calorimetry. Note that the chymotrypsin inhibitors from the hemolymph of silkworm larva (*Bombyx mori*) (32) and from the venom of *Vipera ammodytes ammodytes* (33) possess dissociation constants of 4.3×10^{-9} and 1.3×10^{-8} M, respectively.

CD spectra at different temperatures and pH values demonstrated that BF9 is a protein of high thermostability and that its conformation is independent of pH in the range of 3.0–7.0. It is noteworthy that the results from secondary structure estimation by CD (as shown in Table I) are very close to those from structural analysis by NMR, as described below.

The three-dimensional solution structure of BF9 is shown to be composed mainly of a double-stranded antiparallel β-sheet and a C-terminal α-helix. A one-residue β-strand was observed at Phe^{47} based on NOE connectivities and amide proton exchange rates. We found a β-turn structure at Ser^{27}–His^{30}, which connects the two major β-strands. Based on its three-dimensional structure, the unusual chemical shifts we observed for BF9 were due to an aromatic ring current effect. The upfield shifts for the $C^{\alpha}H$ resonance of Ile^{50} and Cys^{53} are due to the ring current effect of Phe^{23} and Phe^{47}, respectively. The aromatic ring of Tyr^{24} is the major factor that causes the unusual chemical shifts for Pro^{11}. The aromatic ring of Phe^{47} causes the downfield shift of the Tyr^{25} amide proton. Moreover, these aromatic residues form a very rigid hydrophobic core in BF9. The sequence alignment in Fig. 1 shows that the residue corresponding to Phe^{23} in BF9 in other proteins also possesses an aromatic residue, with the exception of a charged residue (Glu) in TAP. It is likely that this charged residue causes some change in the location and environment of the hydrophobic core in TAP. Consequently, the orientations of aromatic residues are different, and the unusual chemical shifts are hence not observed in TAP.

To further evaluate the structural differences among the proteins in the BPTI-like superfamily, we also compared the amide proton exchange rates of BF9 with those reported for five other proteins in the BPTI-like superfamily, as shown in Fig. 10. These exchange rates were all determined under acidic conditions (pH 3.0~5.2) and at temperatures between 30 and 38 °C. We have used these data to compare the structural differences among the different proteins. Interestingly, the medium and slow exchanging amide protons in these proteins are all located in the N-terminal 3_{10} α-helix, β-sheet, and C-terminal α-helix regions, with a few located close to the secondary structure, similar to BF9.

The exchange data are in good agreement with the formation of the C-terminal α-helix for all proteins. In the N-terminal turn-like or 3_{10} α-helix regions, two residues possess slow exchange rates in four (BF9, BPTI, calcicludine, and TAP) of six

TABLE II

^{1}H chemical shifts for BF9 in aqueous solution at 310 K and pH 3.0, using 2,2-dimethyl-2-silapentane-5-sulfonate resonance (0.00 ppm) as a reference

Residue	Chemical shift				
	NH	$C^{\alpha}H$	$C^{\beta}H$	$C^{\gamma}H$	Others
			ppm		
Lys^{1}		4.02	1.92, 1.92	1.48, 1.48	$C^{\delta}H_2$, 1.74, 1.74; $C^{\varepsilon}H_2$, 3.03, 3.03
Asn^{2}	8.71	4.73	2.68, 2.77		
Arg^{3}	8.28	4.25	1.63, 1.63	1.41, 1.47	$C^{\delta}H_2$, 2.85, 3.03; $N^{\varepsilon}H$, 7.01
Pro^{4}		4.27	0.90, 0.90	1.72, 1.90	$C^{\delta}H_2$, 3.54, 3.78
Thr^{5}	8.52	3.87	3.87	1.32	
Phe^{6}	7.13	4.55	3.10, 3.22		$C^{\delta}H_2$, 7.01, 7.01; $C^{\varepsilon}H_2$, 7.41, 7.41; $C^{\zeta}H$, 7.36
Cys^{7}	7.21	4.35	2.06, 2.80		
Asn^{8}	7.45	4.98	2.76, 3.04		$N^{\delta}H_2$, 6.86, 7.48
Leu^{9}	7.45	4.39	1.92, 1.92	1.64	$C^{\delta}H_3$, 0.95, 1.06
Leu^{10}	8.30	4.36	1.47, 1.62	1.85	$C^{\delta}H_3$, 0.99, 0.99
Pro^{11}		4.28	0.24, 0.47	0.38, 0.67	$C^{\delta}H_2$, 3.06, 3.36
Glu^{12}	7.49	4.74	1.75, 2.02	2.33, 2.33	
Thr^{13}	8.92	4.49	4.32	1.40	
Gly^{14}	8.55	4.03, 4.31			
Arg^{15}	8.17	4.43	1.76, 1.91	1.62, 1.62	$C^{\delta}H_2$, 3.18, 3.18; $N^{\varepsilon}H$, 7.13
Cys^{16}	8.56	4.55	2.80, 3.35		
Asn^{17}	8.04	4.81	2.70, 2.81		$N^{\delta}H_2$, 6.73, 7.41
Ala^{18}	8.00	4.31	1.20		
Leu^{19}	7.82	4.35	1.40, 1.53	1.26	$C^{\delta}H_3$, 0.71, 0.82
Ile^{20}	8.40	4.54	1.97	0.94, 0.94	$C^{\delta}H_3$, 1.05; $C^{\gamma}H_3$, 1.40
Pro^{21}		4.56	1.88, 2.13	1.99, 2.22	$C^{\delta}H_2$, 3.74, 3.83
Ala^{22}	8.52	4.55	0.97		
Phe^{23}	9.17	5.86	2.75, 2.88		$C^{\delta}H_2$, 6.82, 6.82; $C^{\varepsilon}H_2$, 7.38, 7.38; $C^{\zeta}H$, 7.36
Tyr^{24}	9.69	5.23	2.71, 2.75		$C^{\delta}H_2$, 6.92, 6.92; $C^{\varepsilon}H_2$, 6.61, 6.61
Tyr^{25}	10.55	4.30	2.74, 3.60		$C^{\delta}H_2$, 7.19, 7.19; $C^{\varepsilon}H_2$, 6.34, 6.34
Asn^{26}	7.89	4.65	2.15, 2.95		$N^{\delta}H_2$, 7.32, 7.72
Ser^{27}	8.44	3.77	4.03, 4.03		
His^{28}	8.12	4.45	3.35, 3.35		$C^{\delta 2}H$, 7.28, $C^{\varepsilon 1}H$, 8.62
Leu^{29}	7.29	4.17	1.44, 1.47	1.13	$C^{\delta}H_3$, 0.75, 0.83
His^{30}	7.75	3.92	3.34, 3.52		$C^{\delta 2}H$, 7.20; $C^{\varepsilon 1}H$, 8.56
Lys^{31}	7.05	4.67	1.58, 1.78	1.11, 1.11	$C^{\delta}H_2$, 1.18, 1.18; $C^{\varepsilon}H_2$, 2.94, 2.94
Cys^{32}	8.99	5.45	2.61, 3.50		
Gln^{33}	9.27	4.82	1.63, 1.63	2.05, 2.14	$N^{\varepsilon}H_2$, 6.91, 7.59
Lys^{34}	8.42	4.82	1.62, 1.69	0.98, 0.98	$C^{\delta}H_2$, 1.19, 1.19; $C^{\varepsilon}H_2$, 2.90, 2.90
Phe^{35}	9.33	4.85	3.04, 3.19		$C^{\delta}H_2$, 7.02, 7.02; $C^{\varepsilon}H_2$, 7.13, 7.13; $C^{\zeta}H$ 6.86
Asn^{36}	8.34	4.85	2.21, 2.60		$N^{\delta}H_2$, 6.75, 7.34
Tyr^{37}	8.84	4.73	2.39, 2.66		$C^{\delta}H_2$, 7.27, 7.27; $C^{\varepsilon}H_2$, 6.72, 6.72
Gly^{38}	8.44	3.44, 4.23			
Gly^{39}	8.02	4.20, 4.20			
Cys^{40}	7.72	4.89	3.10, 3.53		
Gly^{41}	8.97	3.90, 4.01			
Gly^{42}	8.70	3.84, 4.38			
Asn^{43}	8.63	4.82	2.78, 3.07		$N^{\delta}H_2$, 7.61, 7.80
Ala^{44}	7.85	3.91	0.61		
Asn^{45}	7.96	4.86	2.99, 3.18		$N^{\delta}H_2$, 7.90, 7.91
Asn^{46}	6.55	4.85	2.44, 2.44		$N^{\delta}H_2$, 6.82, 7.18
Phe^{47}	9.78	5.02	2.74, 3.33		$C^{\delta}H_2$, 7.28, 7.28; $C^{\varepsilon}H_2$, 7.80, 7.80; $C^{\zeta}H$, 7.59
Lys^{48}	8.95	4.63	2.09, 2.09	1.75, 1.78	$C^{\delta}H_2$, 1.64, 1.64; $C^{\varepsilon}H_2$, 3.07, 3.07
Thr^{49}	7.31	4.83	4.47	1.24	
Ile^{50}	8.16	3.05	0.65	0.91, 1.00	$C^{\delta}H_3$, 0.76; $C^{\gamma 2}H_3$, 0.76
Asp^{51}	7.84	4.28	2.58, 2.63		
Glu^{52}	7.58	3.92	2.25, 2.25	2.56, 2.56	
Cys^{53}	6.94	1.89	2.92, 3.22		
Gln^{54}	8.61	3.70	1.96, 2.16	2.32, 2.55	$N^{\varepsilon}H_2$, 6.77, 7.16
Arg^{55}	8.11	3.92	1.71, 1.78	1.53, 1.53	$C^{\delta}H_2$, 3.11, 3.11; $N^{\varepsilon}H$, 7.25
Thr^{56}	7.47	4.03	3.92	1.56	
Cys^{57}	7.83	4.66	1.90, 2.19		
Ala^{58}	7.61	4.28	1.43		
Ala^{59}	7.85	4.18	1.27		
Lys^{60}	7.92	4.19	1.60, 1.65	1.29, 1.29	
Tyr^{61}	8.04	4.59	2.86, 3.12		$C^{\delta}H_2$, 7.02, 7.02; $C^{\varepsilon}H_2$, 7.13, 7.13
Gly^{62}	8.19	3.93, 3.93			
Arg^{63}	7.84	4.23	1.74, 1.85	1.63, 1.63	$C^{\delta}H_2$, 3.18, 3.18; $N^{\varepsilon}H$, 7.13
Ser^{64}	8.49	4.46	3.92, 3.92		
Ser^{65}	8.35	4.51	3.90, 3.90		

proteins. This indicates the flexibility of the N-terminal region in BPTI-like superfamily proteins. In the antiparallel β-sheet, TAP possesses a distinct exchange rate phenomenon and contains more residues with fast exchange rates. Therefore, it seems that the β-sheet in TAP is less stable than that in the other proteins. In the BF9 β_2-strand, Tyr^{37} displays a fast exchange rate, whereas the corresponding residue in other BPTI-like proteins shows a slow exchange rate. Moreover, we observed a very broad NMR resonance line width of the amide proton of Tyr^{37} in BF9, and no hydrogen bond was detected in the backbone atoms of Tyr^{37} in any of the 10 NMR structures. These observations indicate that Tyr^{37} is not located in the

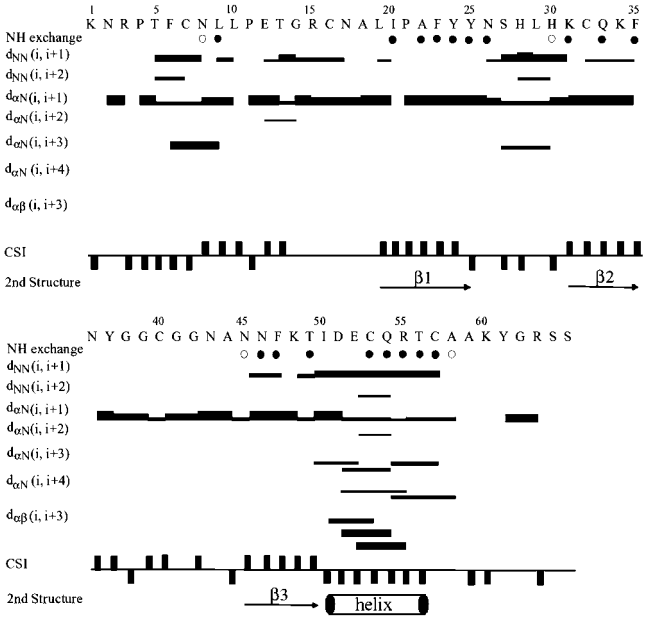

FIG. 6. **Summary of the amide proton exchange rates, NOE connectivities, C$^{\alpha}$H proton chemical shift index, and derived secondary structures.** *Open* and *closed circles* represent medium and slow exchanging amide protons, respectively. *Bar thickness* indicates the intensity of NOE connectivity, with *thicker bars* representing stronger NOEs. *Negative bars* in the chemical shift index (*CSI*) indicate upfield shifts of >0.1 ppm of the C$^{\alpha}$H proton compared with the expected random-coil C$^{\alpha}$H proton chemical shift. *Positive bars* indicate downfield shifts of >0.1 ppm of the C$^{\alpha}$H proton compared with the expected random-coil C$^{\alpha}$H value.

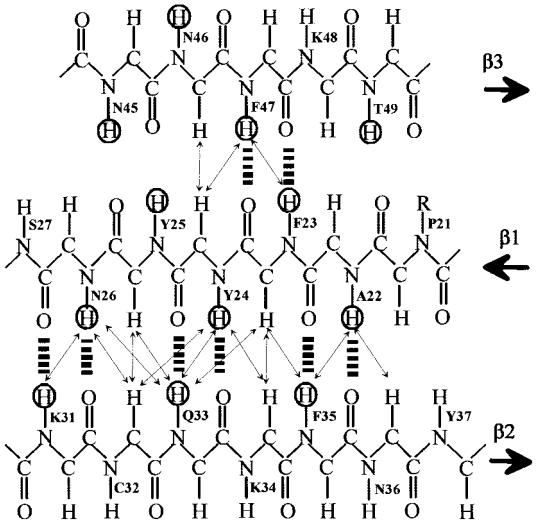

FIG. 7. **Definition of the β-sheet structure of BF9 is shown based on the NOEs and amide proton exchange rate.** Long-range NOEs between β-strands are shown by *double-headed arrows*. *Dashed lines* between backbone amide protons and backbone carbonyl oxygens indicate hydrogen bonds consistent with slow exchanging H^{N} observed in D_2O. The amide protons with slow exchange rates are *circled*.

β_2-strand and is instead at the edge of this strand. In contrast, the backbone amide proton of Asn^{45} in BF9 possesses a medium exchange rate, whereas the corresponding protons in all other proteins show a fast exchange rate. This suggests that the local structures of Asn^{45} and its nearby conformation in BF9 as compared with the other proteins are different. In the β-turn (Ser^{27}–His^{30} in BF9), the corresponding residues in BPTI and TAP all show a fast exchange rate. Most of the residues in this turn region are also small residues (Gly and Ala) in BPTI and TAP. Thus, the β-turn in BPTI and TAP is likely more flexible.

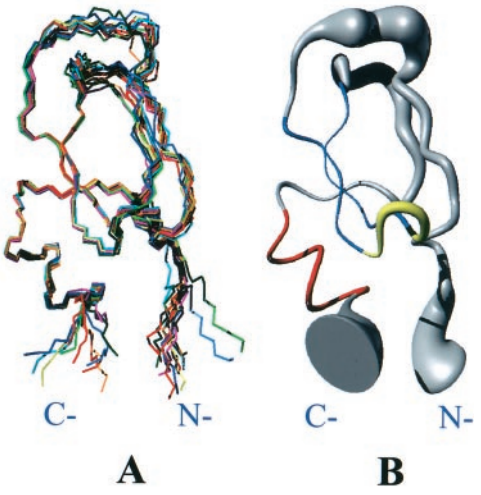

FIG. 8. *A*, superimposition of the backbone atoms (N, C$^{\alpha}$, C′, and O) of 10 NMR structures obtained from simulated annealing and energy minimization calculations. The structures are best fitted to residues 21–26, 31–36, and 50–57. *B*, ribbon structure of the mean NMR solution structure of BF9. A spline function was drawn through the C$^{\alpha}$ atoms, and the radius of the cylindrical rod corresponds to the mean of the global displacements. Only residues 2–60 are shown in both structures.

TABLE III
Structural statistics of the final set of 10 simulated annealing structures of BF9

A. Constraints used	
Distance restraints	
Intra-residue	127
Sequential	172
Medium-range	65
Long-range	153
Total distance	517
Hydrogen bonds	16 × 2
Dihedral angles	33
B. Statistics for the final X-PLOR structures	
Number of structures in the final set	10
X-PLOR energy (kcal/mol)[a]	
E_{NOE}	25.53 ± 1.36
E_{cdih}	14.80 ± 1.28
$E_{bond} + E_{angle} + E_{improper}$	215.51 ± 5.03
E_{elec}	2.13 ± 0.10
E_{VDW}	107.15 ± 1.41
NOE violations	
No. >0.5 Å	None
r.m.s.[b] deviation (Å)	0.048
Deviation from idealized covalent geometry	
Angle (°)	7.79 ± 0.43
Impropers (°)	0.52 ± 0.02
Bonds (Å)	0.005
Mean global r.m.s. deviation (Å)	
Backbone (N, C$^{\alpha}$, C′)	
Residues 21–26, 31–36, 50–57	0.47 ± 0.36
Residues 3–58	0.86 ± 0.23
Heavy atoms	
Residues 21–26, 31–36, 50–57	1.26 ± 0.23
Residues 3–58	1.64 ± 0.38
Ramachandran data	
Residues in most favored regions (%)	68.3
Residues in allowed regions (%)	28.7
Residues in generously allowed regions (%)	2.0
Residues in disallowed regions (%)	0.9

[a] E_{cdih}, torsion angle energies; E_{elec}, electrostatic energies; E_{VDW}, van der Waals repulsive emergies.
[b] Root mean square.

Therefore, there are different exchange rates in the well defined secondary structure regions in the BPTI-like superfamily, revealing that the proteins in the BPTI-like family possess different stabilities in their secondary structures and hence distinct denaturing temperatures.

The functional sites of BPTI were found in segments 12–16

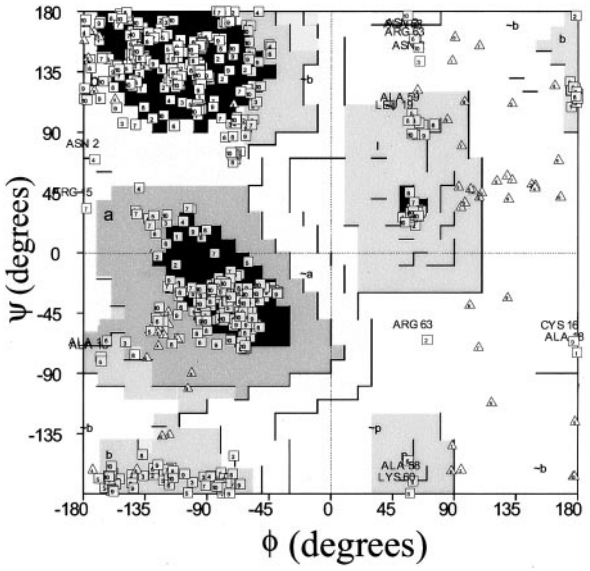

FIG. 9. **Ramachandran plot of ϕ and ψ dihedral angles for the ensemble of 10 NMR structures of BF9 generated using the PROCHECK-NMR program.** *Triangles* in the plots represent the angles for glycine residues.

TABLE IV
List of backbone–backbone hydrogen bonds identified in >30% of the BF9 structures, as calculated by insight II

NH donor	O acceptor	Conformers	2nd structure
Asn^{8}	Thr^{5}	10	3_{10} α-helix
Leu^{9}	Phe^{6}	3	3_{10} α-helix
Ala^{22}	Ile^{20}	10	
Phe^{23}	Phe^{47}	10	β-Sheet
Tyr^{24}	Gln^{33}	10	β-Sheet
Asn^{26}	Lys^{31}	10	β-Sheet
His^{30}	Asn^{26}	7	β-Hairpin
His^{30}	Ser^{27}	4	β-Hairpin
Gln^{33}	Tyr^{24}	10	β-Sheet
Phe^{35}	Ala^{22}	10	β-Sheet
Phe^{47}	Phe^{23}	9	β-Sheet
Lys^{53}	Thr^{49}	5	
Gln^{54}	Ile^{50}	10	α-Helix
Gln^{54}	Asp^{51}	5	
Arg^{55}	Asp^{51}	10	α-Helix
Thr^{56}	Glu^{52}	10	α-Helix
Cys^{57}	Cys^{53}	10	α-Helix

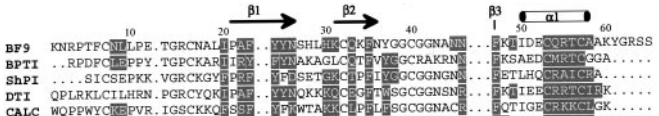

FIG. 10. **Comparison of the amide proton exchange rates of BF9 with the published exchange rate data for the other five protein members of the BPTI superfamily.** The amide protons of the *boxed* residues possess medium or slow exchange rates for BF9 and the corresponding residues in the other proteins. The conditions used for exchange rate experiments were as follows: 37 °C and pH 3.0 for BF9; 36 °C and pH 3.5 for BPTI (38); 36 °C and pH 4.6 for the *S. helianthus* proteinase inhibitor (*ShPI*) (7); 38 °C and pH 5.2 for dendrotoxin I (*DTI*) (12); 30 °C and pH 4.5 for calcicludine (*CALC*) (13); and 36 °C and pH 3.6 for TAP (14). The locations of the secondary structures of BF9 are shown and labeled at the top.

and 36–38, corresponding to Gly^{14}–Ala^{18} and Gly^{38}–Cys^{40} in BF9. These functional residues are all located in the loop regions and possess fast exchange rates. Different active-site residues were identified in BPTI-like toxins. For example, the toxic site of DTK comprises several positively charged residues in the N terminus (Lys^{3} and Lys^{6}) and Lys^{24}, Lys^{26}, and Lys^{28} in the β-turn (34). For TAP, the first four residues (Tyr^{1}, Asn^{2}, Arg^{3}, and Leu^{4}) in the N terminus are the active-site residues (35). Furthermore, a secondary binding determinant located in the C-terminal α-helix was observed in the complex structure of TAP with bovine factor Xa (36). To gain insight into structure-function relationship of BF9, its three-dimensional structure was compared with those of BPTI, DTK, and TAP, which possess different biological functions. Even though these four proteins possess varied degrees of sequence identity, the well defined secondary structure regions, which consist of the β-sheet and the α-helix, are highly similar, as shown in Fig. 11*A*. Also, the aromatic residues that facilitate protein stabilization by forming a hydrophobic interior are generally conserved in these four proteins. Outside of the regular secondary structure elements, the fold of these four proteins is somewhat different. Because the active-site residues are mostly located in the loop or β-turn regions, as described above, one can postulate that the biological difference in BPTI-like proteins is due to a major change in the surface topology of the solvent-exposed amino acid side chains. As shown in Fig. 11*B*, the β-turn in DTK is more exposed to the aqueous phase and is closer to the N terminus compared with the β-turn in BF9 and BPTI. DTK also contains several positively charged residues in these two regions, whereas BF9 and BPTI do not have this characteristic. Thus, the closer location between the β-turn and the N-terminal region when combined with dense positively charged residues might be a key factor for the unique biological activities of BPTI-like toxins such as DTK. By contrast, for the protease inhibitory activity in BF9 and BPTI, the functional site is located in the two flexible loop regions. The amino acid types in these loop regions likely play an important role in causing different inhibitory activities. The β-turn and loop conformations in TAP are very different from the conformations in BF9 (Fig. 11*C*), BPTI, and DTK. This explains why TAP does not possess protease inhibition and channel blocker activities. In summary, we conclude that the proteins in the BPTI-like su-

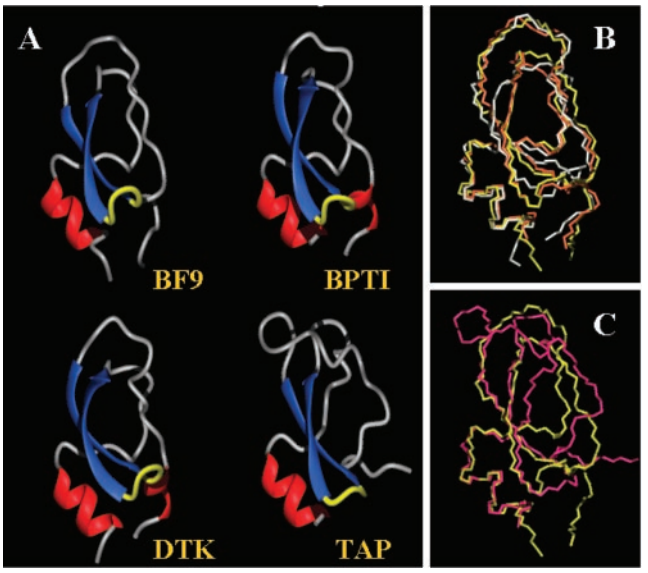

FIG. 11. *A*, ribbon diagrams of BF9, BPTI (accession number PDB-6PTI) (2), DTK (accession number PDB-1DTK) (11), and TAP (accession number PDB-1TAP) (14). The ribbon structures were produced using the MOLMOL program. *B*, pairwise root mean square deviation comparisons of the solution structures of BF9 (*yellow*) and the two homologous proteins, PBB-BPTI (*orange*) and DTK (*white*). The root mean square deviations were calculated for the backbone atoms of residues 4–58, corresponding to residues 2–56 in BPTI and DTK. *C*, pairwise root mean square deviation comparisons of the solution structures of BF9 (*yellow*) and TAP (*red*). The root mean square deviations were calculated for the backbone atoms of residues 31–36 and 50–57 in BF9, corresponding to residues 32–37 and 52–59 in TAP.

perfamily all possess a well defined β-sheet and a C-terminal α-helix secondary structural motif. Because three disulfide bridges are conserved in all BPTI-like proteins, the difference in protein stability among members of the BPTI-like superfamily is mainly due to the distinct stability of the secondary structure region. The biological activity is, however, affected by the types, surface structure, flexibility, and rigidity of the amino acids in the loop regions as well as by the β-turn region.

REFERENCES

1. Wlodawer, A., Walter, J., Huber, H., and Sjolin, L. (1984) *J. Mol. Biol.* **180,** 301–329
2. Wlodawer, A., Nachman, J., Gilliland, G. L., Gallagher, W., and Woodward, C. (1987) *J. Mol. Biol.* **198,** 469–480
3. Berndt, K. D., Guntert, P., Orbons, L. P., and Wüthrich, K. (1992) *J. Mol. Biol.* **227,** 757–775
4. Heald, S. L., Tilton, R. F., Jr., Hammond, L. J., Lee, A., Bayney, R. M., Kamarck, M. E., Ramabhadran, T. V., Dreyer, R. N., Davis, G., Unterbeck, A., and Tamburini, P. P. (1991) *Biochemistry* **30,** 10467–10478
5. Hynes, T. R., Randal, M., Kennedy, L. A., Eigenbrot, C., and Kossiakoff, A. A. (1990) *Biochemistry* **29,** 10018–10022
6. Zweckstetter, M., Czisch, M., Mayer, U., Chu, M. L., Zinth, W., Timpl, R., and Holak, T. A. (1996) *Structure* **4,** 195–209
7. Antuch, W., Berndt, K. D., Chavez, M. A., Delfin, J., and Wüthrich, K. (1993) *Eur. J. Biochem.* **212,** 675–684
8. Dufton, M. J. (1985) *Eur. J. Biochem.* **153,** 647–654
9. Harvey, A. L., and Anderson, A. J. (1991) *Dendrotoxins: Snake Toxins That Block Potassium Channels and Facilitate Neurotransmitter Release in Snake Toxins*, pp. 131–164 Pergamon Press Inc., Tarrytown, New York
10. Skarzynski, T. (1992) *J. Mol. Biol.* **224,** 671–683
11. Berndt, K. D., Guntert, P., and Wüthrich, K. (1993) *J. Mol. Biol.* **234,** 735–750
12. Foray, M. F., Lancelin, J. M., Hollecker, M., and Marion, D. (1993) *Eur. J. Biochem.* **211,** 813–820
13. Gilquin, B., Lecoq, A., Desne, F., Guenneugues, M., Zinn-Justin, S., and Menez, A. (1999) *Proteins Struct. Funct. Genet.* **34,** 520–532
14. Antuch, W., Guntert, P., Billeter, M., Hawthorne, T., Grossenbacher, H., and Wüthrich, K. (1994) *FEBS Lett.* **352,** 251–257
15. Lim-Wilby, M. S., Hallenga, K., de Maeyer, M., Lasters, I., Vlasuk, G. P., and Brunck, T. K. (1995) *Protein Sci.* **4,** 178–186
16. van de Locht, A., Stubbs, M. T., Bode, W., Friedrich, T., Bollschweiler, C., Hoffken, W., and Huber, R. (1996) *EMBO J.* **15,** 6011–6017
17. Liu, C. S., Wu, T. C., and Lo, T. B. (1983) *Int. J. Pept. Protein Res.* **21,** 209–215
18. Laskowski, M., Jr., and Kato, I. (1980) *Annu. Rev. Biochem.* **49,** 593–626
19. Scheidig, A. J., Hynes, T. R., Pelletier, L. A., Wells, J. A., and Kossiakoff, A. A. (1997) *Protein Sci.* **6,** 1806–1824
20. Sreerama, N., and Woody, R. W. (2000) *Anal. Biochem.* **287,** 252–260
21. Rance, M., Sorensen, O. W., Bodenhausen, G., Wagner, G., Ernst, R. R., and Wüthrich, K. (1983) *Biochem. Biophys. Res. Commun.* **117,** 479–485
22. Bax, A., and Davis, D. G. (1985) *J. Magn. Reson.* **65,** 355–360
23. Kumar, A., Ernst, R. R., and Wüthrich, K. (1980) *Biochem. Biophys. Res. Commun.* **95,** 1–6
24. Marion, D., and Wüthrich, K. (1983) *Biochem. Biophys. Res. Commun.* **113,** 967–974
25. Piotto, M., Saudek, V., and Sklenar, V. (1992) *J. Biomol. NMR* **2,** 661–665
26. Hyberts, S. G., Marki, W., and Wagner, G. (1987) *Eur. J. Biochem.* **164,** 625–635
27. Brünger, A. T. (1998) *X-PLOR*, Version 98, Yale University Press, New Haven, CT
28. Koradi, R., Billeter, M., and Wüthrich, K. (1996) *J. Mol. Graph.* **14,** 29–32
29. Nicholls, A., Sharp, K. A., and Honig, B. (1991) *Proteins Struct. Funct. Genet.* **11,** 281–296
30. Laskowski, R. A., Rullmannn, J. A., MacArthur, M. W., Kaptein, R., and Thornton, J. M. (1996) *J. Biomol. NMR* **8,** 477–486
31. Wüthrick, K. (1986) *NMR of Protein and Nucleic Acids*, pp. 130–161, Wiley-Interscience, New York
32. Sasaki, T., and Kobayashi, K. (1984) *J. Biochem.* (*Tokyo*) **95,** 1009–1017
33. Ritonja, A., Meloun, B., and Gubensek, F. (1983) *Biochim. Biophys. Acta* **746,** 138–145
34. Smith, L. A., Reid, P. F., Wang, F. C., Parcej, D. N., Schmidt, J. J., Olson, M. A., and Dolly, J. O. (1997) *Biochemistry* **36,** 7690–7696
35. Dunwiddie C. T., Neeper, M. P., Nutt, E. M., Waxman, L., Smith, D. E., Hofmann, K. J., Lumma, P. K., Garsky, V. M., and Vlasuk, G. P. (1992) *Biochemistry.* **31,** 12126–12131
36. Wei, A., Alexander, R. S., Duke, J., Ross, H., Rosenfeld, S. A., and Chang, C. H. (1998) *J. Mol. Biol.* **283,** 147–154
37. Sorensen, M. D., Bjorn, S., Norris, K., Olsen, O., Petersen, L., James, T. L., and Led, J. J. (1997) *Biochemistry* **36,** 10439–10450
38. Wagner, G., and Wüthrich, K. (1982) *J. Mol. Biol.* **160,** 343–361